International Journal of Remote Sensing
Vol. 28, No. 10, 20 May 2007, 2383–2390

Change analysis of land surface temperature based on robust statistics in the estuarine area of Pearl River (China) from 1990 to 2000 by Landsat TM/ETM+ data

J. ZHANG†‡, Y. WANG*‡ and Z. WANG§

†Computer School, South China Normal University, Guangzhou, 510631, China
‡State Key Laboratory of Organic Geochemistry, Guangzhou Institute of Geochemistry, Chinese Academy of Sciences, Guangzhou, 510640, China
§Faculty of Science and Technology, University of Macau, Macao, China

(*Received 19 August 2006; in final form 31 December 2006*)

The estuarine area of Pearl River that has taken great changes in land cover since 1990 is a typical area for studying the change of land surface temperature (LST). The LST of the years 1990 and 2000 in this area was estimated from the data of Landsat TM/ETM+ band 6, respectively, and three scales, corresponding to high, normal and low temperature ranges, were divided by a robust statistical method. The results show that the area of high temperature range in 2000 has an increase of 250 km^2 compared with the year 1990. The urban-used land and the bare land are the main land cover types constituting the high temperature range area.

1. Introduction

As one of the important factors that affect the global climate change and energy balance near the ground surface, land surface temperature (LST) has been paid more and more attention. Traditionally, temperature data for an urban heat island (UHI) are mainly collected from weather stations or gathered along traverses with thermometers mounted on automobiles, which proves to be extremely hard to acquire the detailed spatial distribution of temperature. With the development of remote sensing technology, surface temperatures can be acquired effortlessly and many researches have been conducted using thermal remote sensing technology. Streutker (2003) studied the growth of surface urban heat island (S-UHI) of Houston in a 12-year interval using the infrared channels of the Advanced Very High Resolution Radiometer (AVHRR). Weng (2003) performed a fractal analysis of UHI of the city of Guangzhou by using Landsat TM data for different years. Some other researchers investigated the impact of UHI and found many related factors, which affected the UHI, such as the vegetation abundance (Boegh *et al.* 1998, Carson *et al.* 1994, Lo *et al.* 1997), soil moisture and roughness of the land surface (Friendl 2002). Remote sensing technology has also been used to study the climate change (Kalnay and Cai 2003, Voogt and Oke 2003) and energy balance between bottom of the atmosphere and ground surface (Lo *et al.* 1997).

Here, we focus on the LST changes in the estuarine area of Pearl River in 1990 and 2000, respectively. The main objectives are (1) estimating high temperature area

*Corresponding author. Email: wangyp@gig.ac.cn

International Journal of Remote Sensing
ISSN 0143-1161 print/ISSN 1366-5901 online
http://www.tandf.co.uk/journals
DOI: 10.1080/01431160701236811

(HTA) using a robust statistical method and analyzing its changes; and (2) summarizing the change properties of the land cover in this area and exploring their contribution to HTA's increase.

2. Study area

The study area is in the south of Guangdong, China (N 22.4–23.4°, E 113–114°), enjoying a subtropical climate. The average annual temperature is between 18.7 and 23.4°C, with an average annual rainfall of 1500–2000 mm. This area has experienced great changes in the past 20 years and undergone a quick urbanization process since the 1980s. With the quick progress of the economy, especially the rapid industrialization, a great amount of agricultural land has been converted into construction area and development sites and urban land afterwards (Li and Yeh 2004).

3. Materials and methods

3.1 *Image data and pre-processing*

Two scenes of Landsat TM/ETM + image, date 13 October 1990 and 1 November 2000, were acquired. A systematical geometric and radiometric correction were performed to the image data using the calibration parameter file (CPF) released by the Earth Resources Observation Systems Data Center, United States Geological Survey, before the delivery. The Landsat TM image of the year 1990 was further registered to the ETM + image of the year 2000 with the resultant root mean square error being less than 0.5 pixels, so that both TM/ETM + images of the two years had same spatial resolution and covered the same area.

3.2 *Image classification*

Eight classes for both years were classified respectively from the TM (1990) and ETM + (2000) images by using bands 1–5 and 7 and the classes include: (1) old urban land, (2) new urban land, (3) sand land and construction sites, (4) woodland, (5) cropland, (6) bare land, (7) water, (8) dike–pond. The old and new urban land was mainly determined by the age of the buildings and their spectral characteristics. In the study, supervised classification with the maximum likelihood algorithm was performed to classify the Landsat 7 TM/ETM + images. The accuracy for each classification map was checked with the random sampling method and 25 samples were selected for each land cover category to check the ground truth. The reference data were collected either from field survey or from the published land cover maps. The average accuracy of classification and the Kappa coefficients were determined to be 78% and 0.817 for 1990 and 81.5% and 0.82 for 2000, respectively.

3.3 *Retrieving land surface temperature*

The signals received by the thermal sensors can be converted to at-sensor radiance (L_λ) using equation (1):

$$L_\lambda = \text{gain} \times DN + \text{offset} \tag{1}$$

where L_λ is the radiance of the thermal band pixels in W $(\text{m}^2 \cdot \text{ster} \cdot \mu\text{m})^{-1}$, gain is the

slope of the radiance/*DN* conversion function, *DN* is the digital number of a given pixel, and offset is the intercept of the radiance/*DN* conversion function (Landsat Project Science Office 2002). The gain and offset values can be found in the metadata of the TM/ETM+ image.

The radiance values from the TM/ETM+ thermal band were then transformed to radiant surface temperature, namely brightness temperature, using thermal calibration constants supplied by the Landsat Project Science Office (2002) according to equation (2):

$$T_6 = \frac{K_2}{\ln\left(\frac{K_1}{L_\lambda} + 1\right)} \tag{2}$$

where T_6 is the at-sensor brightness temperature in K, K_1 and K_2 are the pre-launch calibration constants (for Landsat 7 ETM+: $K_1 = 666.09\,\mathrm{W}\ (\mathrm{m}^2\,\mathrm{ster}\,\mu\mathrm{m})^{-1}$ and $K_2 = 1282.71\,\mathrm{K}$; for Landsat 5 TM, $K_1 = 607.76\,\mathrm{W}\ (\mathrm{m}^2\,\mathrm{sr}\,\mu\mathrm{m})^{-1}$, and $K_2 = 1260.56\,\mathrm{K}$).

To obtain a reasonably high-quality LST, the mono-window algorithm of Qin *et al.* was used here. Only three parameters were required for the algorithm: emissivity, transmittance and effective mean atmospheric temperature (Qin *et al.* 2001). The algorithm was as follows:

$$T_s = \frac{a_6(1 - C_6 - D_6) + [b_6(1 - C_6 - D_6) + C_6 + D_6]T_6 - D_6 T_a}{C_6} \tag{3}$$

where T_s is the land surface temperature; T_6 is the brightness temperature from equation (2); T_a is the effective mean atmospheric temperature; a_6 is $-67.355351$and b_6 is 0.458606 when the LST is between 0 and 70°C (Qin *et al.* 2001); C_6 and D_6 can be calculated using following equations:

$$C_6 = \varepsilon_6 \tau_6 \tag{4}$$

$$D_6 = (1 - \tau_6)[1 + (1 - \varepsilon_6)\tau_6] \tag{5}$$

where ε_6 is the ground surface emissivity and τ_6 is the atmospheric transmittance; T_a, ε_6, τ_6 are the three parameters needed to covert the brightness temperature to LST. τ_6 could be estimated according to the near-surface air temperature and the water vapour concentration from the local meteorological observatories and it was found that there is a linear relationship between τ_6 and water vapour. Table 1 shows the equations for estimation of atmospheric transmittance at different water vapour conditions (Qin *et al.* 2001). The effective mean atmospheric temperature (T_a) was calculated using equation (6):

$$T_a = 17.9769 + 0.91715T_0 (\text{for tropical area}) \tag{6}$$

Table 1. Estimation of atmospheric transmittance for Landsat TM/ETM+ Band 6 (Qin *et al.* 2001).

Water vapor (w)($\mathrm{g\,cm^{-2}}$)	Transmittance estimation equation
0.4–1.6	$\tau_6 = 0.974290 - 0.08007w$ (High air temperature) $\tau_6 = 0.982007 - 0.09611w$ (Low air temperature)
1.7–3.0	$\tau_6 = 1.031412 - 0.11536w$ (High air temperature) $\tau_6 = 1.053710 - 0.14142w$ (Low air temperature)

where T_a is the effective mean atmospheric temperature; T_0 is the near-surface air temperature that could be acquired from the local meteorological observatories. More detailed information about the linear equations can be found in the paper by Qin *et al.* (2001).

Ground surface emissivity is very critical in determining the surface temperature, but is particularly hard to measure as it is affected by a variety of factors such as ground wetness, structure and roughness, etc (Gillespie *et al.* 1998). In some studies, ground surface emissivity was estimated by the NDVI value with a threshold established to the NDVI image (Valor and Caselles 1996, Van de Griend and Owe 1993, Weng 2001, 2003). It seems more appropriate to correct the effect of emissivity on LST derived from thermal remote sensing image by assigning an emissivity value to each land cover category of the classification image (Watson 1992, Snyder *et al.* 1998). Each land cover type was assigned an emissivity value (table 2) according to the previous studies, which ranges from 0.950 to 0.99 (Humes *et al.* 1994, Nichol 1994, Snyder *et al.*, 1998). Retrieving the land surface temperature was finished through a C++ program by Zhang *et al.* (2006).

3.4 *Quantification of LST based on robust statistics*

Streutker (2002) took a Gaussian-based density slice method to quantify LST data for comparing the data of different years. Here, a robust statistical method is proposed to divide the LST into high, normal and low temperature ranges. Robust statistics is a family of theories and techniques for estimating the parameters of a parametric model while dealing with deviations from idealized assumptions (Hampel *et al.* 1986).

Figure 1 shows the histogram distribution of LST images for both 1990 and 2000. It is found that the LST images follow a normal distribution; that is to say, the robust statistics can be applied. Most of the pixels are located in the range of average temperature $\pm$ one standard deviation (sd). These pixels are considered as normal temperature area. The area with surface temperature above average temperature + one sd would be defined as the high temperature area. Contrarily, the area with surface temperature lower than average temperature $\pm$ one sd would be defined as the low temperature area. Here, the average temperature $\pm$ one sd are set as two threshold values that divide the LST into three ranges. By calculating the pixel numbers in each range, the area of each temperature range would be quantified.

4. Results and analysis

Figures 2 and 3 show the LST results of the study area in 1990 and 2000 estimated from TM/ETM+ data. It was found that there was a great change from 1990 to 2000. The LST of the eastern and western shores along Pearl River were always the same in 1990, but the LST of the eastern shore is obviously higher than that of the

Table 2. Emissivity values for every land cover type.

Land types	Old urban land	Wood land	Water	Bare land	Dike–pond	New urban land	Sand land and construction sites	Cropland
Emissivity values	0.961	0.980	0.990	0.953	0.988	0.956	0.950	0.971

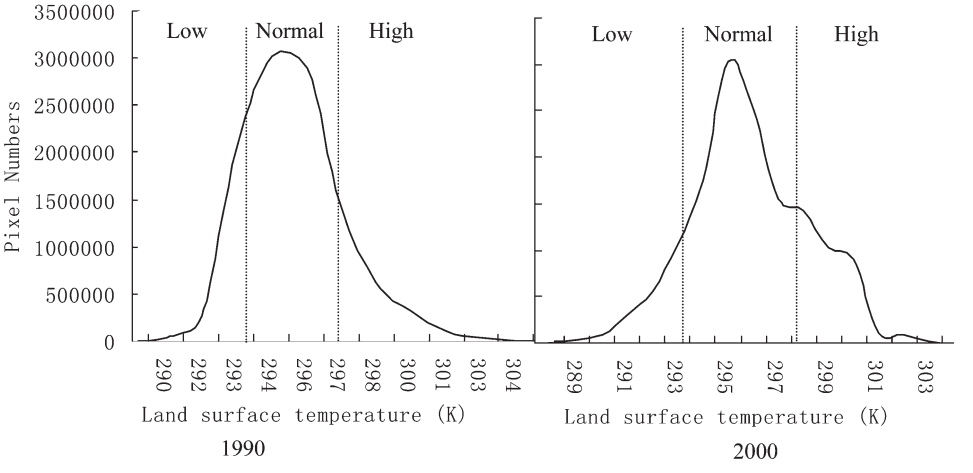

Figure 1. Histogram distribution of LST images for both 1990 and 2000.

western shore in 2000. In 1990, the high temperature area was mainly located in the surrounding area of Guangzhou and the bare ground area north of Guangzhou. There is no distinct difference between the eastern and western shores of the estuarine area of Pearl River. Whereas in 2000, besides the high temperature area in the surrounding area of Guangzhou, the eastern shore of estuarine area of Pearl River was almost covered by high temperature area. By comparing the average temperature of the two shores, the average temperature of the eastern shore was about 1.6°C higher than that of the western shore.

4.1 *Temporal and spatial change of LST*

According to the method in §3.4, the average temperatures (AT) and standard deviations (sd) of two years are computed, which are AT=295.8 K and sd=1.9 for 1990 and AT=296.0 K and sd=2.3 for 2000, respectively. The segment results of three temperature areas and their changes of each temperature range from 1990 to 2000 are

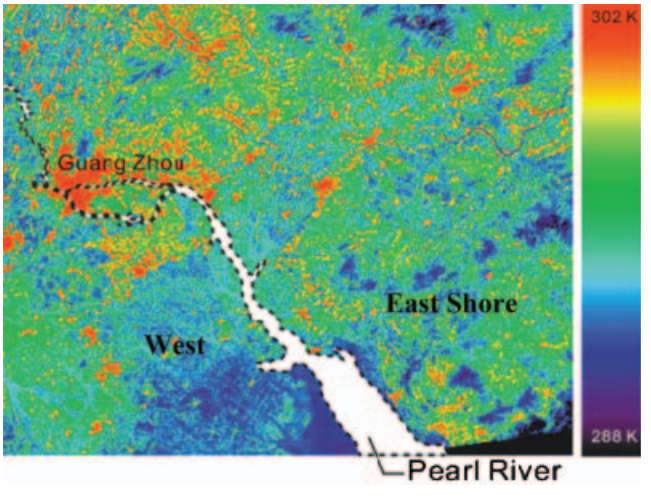

Figure 2. LST image in the Pearl River delta in the year 1990.

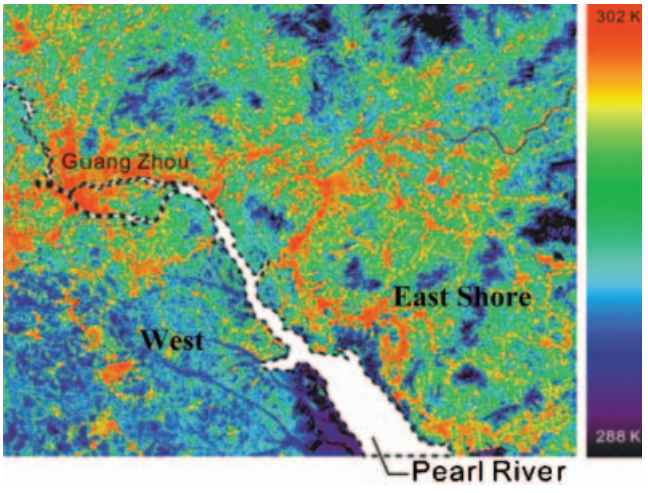

Figure 3. LST image in the Pearl River delta in the year 2000.

listed in table 3. It can be found that the high temperature area exhibits a big increase, which is about 250 km^2 from 1990 to 2000, while the area of low temperature area is decreasing. The changes of high temperature area and low temperature area reflect the trend of temperature change in the estuarine area of Pearl River.

4.2 *Land cover component of the high temperature area*

By performing overlap analysis to the LST images and classification maps, respectively, for both 1990 and 2000, the land cover components of the high temperature area were estimated respectively, which are listed in table 4. It can be found that the bare ground land is the main component in the year of 1990. It takes a percentage of 41.4%. The urban-used land is in the second place including both the old urban land and new urban land, which takes a percentage of 36.1%. In 2000, the main component of the high temperature area is urban-used land with a percentage of 60.9%, and 28.0% for the bare ground land. It can be concluded easily that the urban-use land and the bare ground land are the main components of the high temperature area for both years. It implies that the increase of urban-use land and bare ground land will lead to the increase of the high temperature area.

4.3 *Temperature partition analysis of different land covers*

Table 5 shows the constitution of each land cove in different temperature ranges. It can be found that most of the urban-used land is in the high temperature area for both years. In 1990, 77.1% of the old urban land and 53.1% of the new urban land belong to the high temperature area. In 2000, these proportions were still as high as

Table 3. Area in different temperature scales and their changes from 1990 to 2000 (km^2).

Ranges	Area in 1990	Area in 2000	Total changes	Changes in percentage (%)
High temperature area	1481.13	1731.92	250.79	16.93
Normal temperature area	7477.33	7386.79	−90.54	−1.21
Low temperature area	1774.07	1613.83	−160.24	−9.03

Table 4. Land cover components of high temperature area in 1990 and 2000 (%).

Year	Old urban land	New urban land	Sand land and construction sites	Bare land	Other land
1990	15.4	20.7	1.8	41.4	20.7
2000	29.5	31.4	1.6	28.0	9.5

Table 5. Constitutes of different land cover in three temperature ranges

	Low temperature area (%)		Normal temperature area (%)		High temperature area (%)	
Land cover types	1990	2000	1990	2000	1990	2000
Old urban land	0.3	0.5	22.6	30.3	77.1	69.2
New urban land	0.9	1.2	46.0	46.4	53.1	52.4
Sand land and construction sites	0.8	8.4	44.6	72.1	54.6	19.4
Bare land	0.8	1.0	68.8	76.0	30.4	23.0
Wood land	16.4	44.8	78.8	54.9	4.8	0.3
Water	51.4	42.9	47.4	57.1	1.2	0.0
Dike–pond	7.6	25.2	84.8	71.3	7.6	3.5
Cropland	19.6	6.1	77.7	90.5	2.7	3.4

69.2% and 52.4%. The results indicate that more than half of the urban-used land belongs to the high temperature area for both years. Besides the urban-used land, there are also considerable areas of sand land, construction sites and bare land belonging to the high temperature area. Comparatively, the woodland, water and green cropland are located in the low and normal temperature area. Here, the same land cover may take different percentages in different years, especially for woodland, sand land and construction sites. It is mainly because the great decrease or increase in area of the land-cover types.

5. Conclusion

It should be noted that there still exist some problems for LST study by using thermal remote sensing data, which is only a 'snapshot' at a specific time of a day. More *in situ* information should be integrated well with the thermal remote sensing image data. Further study on the LST by using thermal remote sensing needs to be continued.

Acknowledgements

Supported by Guangdong S&T Project (2005B30801007, 2004A30401001), CAS (KZCX3-SW-224) and Guangdong NSF (04002143). Professor Giles Foody and two anonymous reviewers are thanked for their constructive comments.

References

Boegh, E., Soegaard, H., Hanan, N., Kabat, P. and Lesch, L., 1998, A remote sensing study of the NDVI-Ts relationship and the transpiration from sparse vegetation in the Sahel based on high resolution satellite data. *Remote Sensing of Environment*, **69**, pp. 224–240.

Carson, T.N., Gillies, R.R. and Perry, E.M., 1994, A method to make use of thermal infrared temperature and NDVI measurements to infer surface soil water content and fractional vegetation cover. *Remote Sensing of Environment*, **9**, pp. 161–173.

FRIENDL, M.A., 2002, Forward and inverse modeling of land surface energy balance using surface temperature measurements. *Remote Sensing of Environment*, **79**, pp. 344–354.

GILLESPIE, A.R., ROKUGAWA, S., MATSUNAGA, T., COTHERN, J.S., HOOK, S.J. and KAHLE, A.B., 1998, A temperature and emissivity separation algorithm for advanced spaceborne thermal emission and reflection radiometer (ASTER) images. *IEEE Transactions on Geoscience and Remote Sensing*, **36**, pp. 1113–1126.

HAMPEL, F.R., RONCHETTI, E.M., ROUSSEEUW, P.J. and STAHEL, W.A., 1986, *Robust Statistics, the Approach Based on Influence Functions* (New York: John Wiley & Sons).

HUMES, K.S., KUSTAS, W.P., MORAN, M.S., NICHOLS, W.D. and WELTZ, M.A., 1994, Variability of emissivity and surface temperature over a sparsely vegetated surface. *Water Resources Research*, **30**, pp. 1299–1310.

KALNAY, E. and CAI, M., 2003, Impact of urbanization and land use on climate change. *Nature*, **423**, pp. 528–531.

LANDSAT PROJECT SCIENCE OFFICE 2002, Landsat 7 science data user's handbook. Goddard Space Flight Center. Available online at: http://landsathandbook.gsfc.nasa.gov/handbook.html).

LI, X. and YEH, A.G.O., 2004, Analyzing spatial restructuring of land use patterns in a fast growing region using remote sensing and GIS. *Landscape and Urban Planning*, **69**, pp. 335–354.

LO, C.P., QUATTROCHI, D.A. and LUVALL, J.C., 1997, Application of high-resolution thermal infrared remote sensing and GIS to assess the urban heat island effect. *International Journal of Remote Sensing*, **18**, pp. 287–304.

NICHOL, J.E., 1994, A GIS-based approach to microclimate monitoring in Singapore's high-rise housing estates. *Photogrammetric Engineering and Remote Sensing*, **60**, pp. 1225–1232.

QIN, Z., KARNIELI, A. and BERLINER, P., 2001, A mono-algorithm for retrieving land surface temperature from Landsat TM data and its application to the Israel–Egypt border region. *International Journal of Remote Sensing*, **18**, pp. 583–594.

SNYDER, W.C., WAN, Z., ZHANG, Y. and FENG, Y.-Z., 1998, Classification-based emissivity for land surface temperature measurement from space. *International Journal of Remote Sensing*, **19**, pp. 2753–2774.

STREUTKER, D.R., 2002, A remote sensing study of the urban heat island of Houston, Texas. *International Journal of Remote Sensing*, **23**, pp. 2595–2608.

STREUTKER, D.R., 2003, Satellite-measured growth of the urban heat island of Houston, Texas. *Remote Sensing of Environment*, **85**, pp. 282–289.

VALOR, E. and CASELLES, V., 1996, Mapping land surface emissivity from NDVI: application to European, African, and South American areas. *Remote Sensing of Environment*, **57**, pp. 167–184.

VAN DE GRIEND A.A. and OWE, M., 1993, On the relationship between thermal emissivity and the normalized different vegetation index for natural surfaces. *International Journal of Remote Sensing*, **14**, pp. 1119–1131.

VOOGT, J.A. and OKE, T.R., 2003, Thermal remote sensing of urban climates. *Remote Sensing of Environment*, **86**, pp. 370–384.

WATSON, K., 1992, Spectral ratio method for measuring emissivity. *Remote Sensing of Environment*, **42**, pp. 113–116.

WENG, Q., 2001, A remote sensing–GIS evaluation of urban expansion and its impact on surface temperature in the Zhujiang Delta, China. *International Journal of Remote Sensing*, **22**, pp. 1999–2014.

WENG, Q., 2003, Fractal analysis of satellite-detected urban heat island effect. *Photogrammetric Engineering and Remote Sensing*, **69**, pp. 555–566.

ZHANG, J., WANG, Y. and LI, Y., 2006, A C++ program for retrieving land surface temperature from the data of Landsat TM/ETM+ band6. *Computers & Geosciences*, **32**, pp. 1796–1805.